Thin Solid Films 520 (2012) 2554–2561

Contents lists available at SciVerse ScienceDirect

Thin Solid Films

journal homepage: www.elsevier.com/locate/tsf

Sputter deposition of semicrystalline tin dioxide films

B. Selin Tosun [a], Rebekah K. Feist [b], Aloysius Gunawan [a], K. Andre Mkhoyan [a], Stephen A. Campbell [c], Eray S. Aydil [a,*]

[a] Department of Chemical Engineering and Materials Science, University of Minnesota, 421 Washington Avenue SE, Minneapolis, MN 55455, USA
[b] Dow Solar Solutions, The Dow Chemical Company, 1381 Building, Office 201, Midland, MI 48667, USA
[c] Department of Electrical and Computer Engineering, 200 Union Street SE, Minneapolis, MN 55455, USA

ARTICLE INFO

Article history:
Received 10 June 2011
Received in revised form 29 October 2011
Accepted 31 October 2011
Available online 6 November 2011

Keywords:
Tin dioxide
Semicrystalline
Sputtering
Amorphous
X-ray diffraction
Electrical properties

ABSTRACT

Tin dioxide is emerging as an important material for use in copper indium gallium diselenide based solar cells. Amorphous tin dioxide may be used as a glass overlayer for covering the entire device and protecting it against water permeation. Tin dioxide is also a viable semiconductor candidate to replace the wide band gap zinc oxide window layer to improve the long-term device reliability. The film properties required by these two applications are different. Amorphous films have superior water permeation resistance while polycrystalline films generally have better charge carrier transport properties. Thus, it is important to understand how to tune the structure of tin dioxide films between amorphous and polycrystalline. Using X-ray diffraction (XRD) and Hall-effect measurements, we have studied the structure and electrical properties of tin dioxide films deposited by magnetron sputtering as a function of deposition temperature, sputtering power, feed gas composition and film thickness. Films deposited at room temperature are semicrystalline with nanometer size SnO_2 crystals embedded in an amorphous matrix. Film crystallinity increases with deposition temperature. When the films are crystalline, the X-ray diffraction intensity pattern is different than that of the powder diffraction pattern indicating that the films are textured with (101) and (211) directions oriented parallel to the surface normal. This texturing is observed on a variety of substrates including soda–lime glass (SLG), Mo-coated soda–lime glass and (100) silicon. Addition of oxygen to the sputtering gas, argon, increases the crystallinity and changes the orientation of the tin dioxide grains: (110) XRD intensity increases relative to the (101) and (211) diffraction peaks and this effect is observed both on Mo-coated SLG and (100) silicon wafers. Films with resistivities ranging between 8 mΩ cm and 800 mΩ cm could be deposited. The films are n-type with carrier concentrations in the 3×10^{18} cm^{-3} to 3×10^{20} cm^{-3} range. Carrier concentration decreases when the oxygen concentration in the feed gas is above 5%. Electron mobilities range from 1 to 7 cm^2/V s and increase with increasing film thickness, oxygen addition to the feed gas and film crystallinity. Electron mobilities in the 1–3 cm^2/V s range can be obtained even in semicrystalline films. Initial deposition rates range from 4 nm/min at low sputtering power to 11 nm/min at higher powers. However, deposition rate decreases with deposition time by as much as 30%.

1. Introduction

Thin tin dioxide (SnO_2) films find applications in a wide variety of devices such as sensors and solar cells [1–4]. SnO_2 is a wide band gap (3.8 eV) semiconductor that crystallizes in tetragonal Cassiterrite crystal structure with lattice parameters $a=b=4.737$ Å and $c=3.185$ Å. Although, SnO_2 thin films have been used in gas sensors and as transparent conducting electrodes, its high chemical stability also makes it an attractive replacement for wide band gap semiconductor oxides such as ZnO. Tin dioxide has been deposited on various substrates including Si [1,5], glass slides [2,5–9], quartz [10], InSb [3] and InP [4]. Many techniques such as sol–gel deposition [11], chemical bath deposition from $SnCl_4$[12], chemical vapor deposition [13], spray pyrolysis [14], electron beam evaporation [9,15], thermal evaporation [16] and sputtering [1–8,10,17–19] have been used to deposit SnO_2 films. In most studies where intrinsic SnO_2 was studied, the films have been deposited by reactive sputtering of metallic tin (Sn) target under O_2/Ar atmosphere [1,3–4]. Films deposited at low O_2 concentration in the feed gas show metallic characteristics [1]. In high power DC sputtering, the films consist mostly of the monoxide phase [1,6,8]. Most of the research on sputtered SnO_2 films focused on depositing n-type films with high conductivity by doping with Sb [6–8,10,18–19]. SnO_2:Sb has been studied both with reactive sputtering of Sn:Sb (95.5% weight purity) metallic targets using Ar/O_2 gas [6,8] and with RF sputtering of SnO_2 ceramic targets with Ar gas [7,10,18–19]. Increase in deposition rates, grain sizes, carrier

* Corresponding author. Tel.: +1 612 625 8593; fax: +1 612 626 7246.
E-mail address: Aydil@umn.edu (E.S. Aydil).

0040-6090/$ – see front matter © 2011 Elsevier B.V. All rights reserved.
doi:10.1016/j.tsf.2011.10.169

concentration and carrier mobility have been observed with increasing sputtering power and decreasing working pressure [7]. The lowest resistivity achieved with SnO_2:Sb films in these studies was 2 mΩ cm. SnO_2 has also been deposited in nitrogen ambient to form p-type SnO_2:N [17].

In some applications, it is desirable to use SnO_2 instead of crystalline ZnO. While sputtered ZnO films are almost always crystalline with (0002) axis of the grains oriented normal to the substrate, sputtered SnO_2 films can be crystalline or amorphous with comparable charge densities and mobilities to sputtered ZnO. Since ZnO and SnO_2 also have similar band gaps, amorphous SnO_2 may be a potential replacement for ZnO in copper indium gallium diselenide (CIGS) solar cells. Amorphous SnO_2 may be preferred in applications where water penetration into the layers under the oxide layer reduces the long-term reliability of the devices as is the case in CIGS thin film solar cells. Polycrystalline ZnO is susceptible to water penetration through grain boundary diffusion of water whereas amorphous SnO_2 can act as a barrier. Mixture of amorphous and nanocrystalline SnO_2 where nanocrystals are embedded in amorphous matrix without forming grain boundaries may even achieve better charge transport properties without sacrificing the barrier properties. Thus, it is important to be able to control the structure of SnO_2 films between amorphous and polycrystalline.

In this study, we deposit SnO_2 films using radio frequency (RF) magnetron sputtering and study the effects of RF power, substrate temperature, film thickness and oxygen concentration in the feed gas on the electrical and structural properties of the deposited films. The films' crystal structure was studied by X-ray diffraction (XRD) and transmission electron microscopy (TEM) while electrical properties were determined using a combination of room temperature Hall-effect and four-point probe measurements. This study was conducted to find the sputtering conditions that yield semicrystalline films where nanocrystals of SnO_2 are prevalent but do not abut against each other to form grain boundaries.

2. Experimental details

Tin dioxide films were sputtered from a 3" diameter wide and 0.25" thick SnO_2 (99.99% purity) ceramic target in a AJA-ATC-2000 sputtering system. The substrates were either polycrystalline Mo (250 nm) coated 1 mm thick glass (Mo-SLG) substrates or bare 1 mm thick soda–lime glass (SLG) slides. In some experiments (100) Si wafers were also used. All substrates were cleaned ultrasonically in a deionized water, acetone and isopropanol mixture (1:1:1 ratio by volume) and dried by blowing compressed air across the substrate. The target surface was cleaned for 3 min by presputtering prior to all depositions while a shutter that protects the substrate was closed. The base pressure in the sputtering chamber was around 2.7×10^{-4} Pa and sputtering was started only after reaching this pressure or lower for each experiment. The sputtering pressure was kept constant at 0.67 Pa, which was maintained by flowing 20 sccm of sputtering gasses (Ar or Ar/O_2) into the chamber. The sputtering guns are aligned at an angle of 23.58° with respect to the vertical axis which is normal to the substrate surface. Target to substrate distance was 19.5 cm. The substrate platen was rotated at 20 rpm throughout the deposition and heated using tungsten–halogen infrared lamps beneath the platen.

The RF power and the O_2 concentration in the feed gas were varied for sputtering between 100 W and 250 W and from 0% to 15%, respectively. Films were deposited for different time periods to yield different thicknesses: specifically, we deposited and studied films that were 200 ± 20 nm, 300 ± 20 nm and 500 ± 20 nm thick. In the experiments where O_2 is used, the total flow rate of Ar and O_2 was kept constant at 20 sccm. In the experiments where the substrates were heated to 150 °C, the substrates were kept at 150 °C for 10 min prior to starting the plasma and the deposition.

Film thicknesses were measured using a surface profilometer by scanning through a step between the film and the substrate. This step was created by partially covering the substrate prior to the deposition. Cu-Kα radiation ($\lambda=0.154056$ nm) was used to record XRD from the films and to study the structural properties. A Bruker–AXS microdiffractometer equipped with a 2.2 kW sealed Cu source and a two dimensional Hi-Star detector was used. The 2D detector improves the signal to noise ratio via the collection of both specular and non-specular diffracted X-rays. The X-ray beam spot size was 800 μm. The sheet resistance of the films was determined by both a linear four-point probe system and Hall-effect measurements using the Van-der-Pauw configuration at room temperature. The electrical measurements were done on films deposited on SLG substrates. Transmission electron microscopy (TEM) analysis was conducted using an FEI Tecnai F-30 microscope with a Schottky field-emission electron gun operated at 300 keV [20].

3. Results and discussion

3.1. Effect of RF power on the films' electrical and structural properties

As expected, the film deposition rate increases with increasing RF power. Fig. 1 shows the average deposition rates determined by dividing the film thickness by the deposition time. This increase with increasing RF power is due to increasing argon ion (Ar^+) density and the ensuing increase in the sputtering rate. However, the deposition rate decreases with elapsed deposition time. For example, Fig. 1 shows that the average deposition rate is lower when depositing a 500 nm thick film than when depositing a 200 nm thick film. Fig. 1 also shows that the deposition rate is insensitive to the substrate temperature. This rules out heating of the substrates as the cause for the deposition time dependence of the deposition rate. There could be numerous reasons for sputtering time dependence including heating of the target or changes in the structure and surface of the film, which may affect the sticking properties but this is not a focus of this study.

Fig. 2 shows the XRD from films deposited under a variety of conditions on Mo-coated soda–lime glass. XRD from (110), (101) and (211) Cassiterrite planes are clearly detectable superimposed on broader peaks in some films but are completely absent in others indicating that the crystallinity of the film depends on sputtering conditions and film thickness. First obvious trend is that thicker films tend to appear more crystalline than the thinner films regardless of the deposition temperature. The 200 nm thick films, Fig. 2(a) and

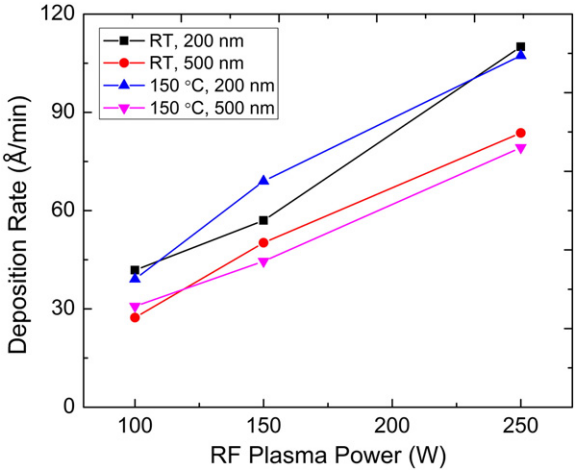

Fig. 1. Time-averaged SnO_2 film deposition rate as a function of RF sputtering power.

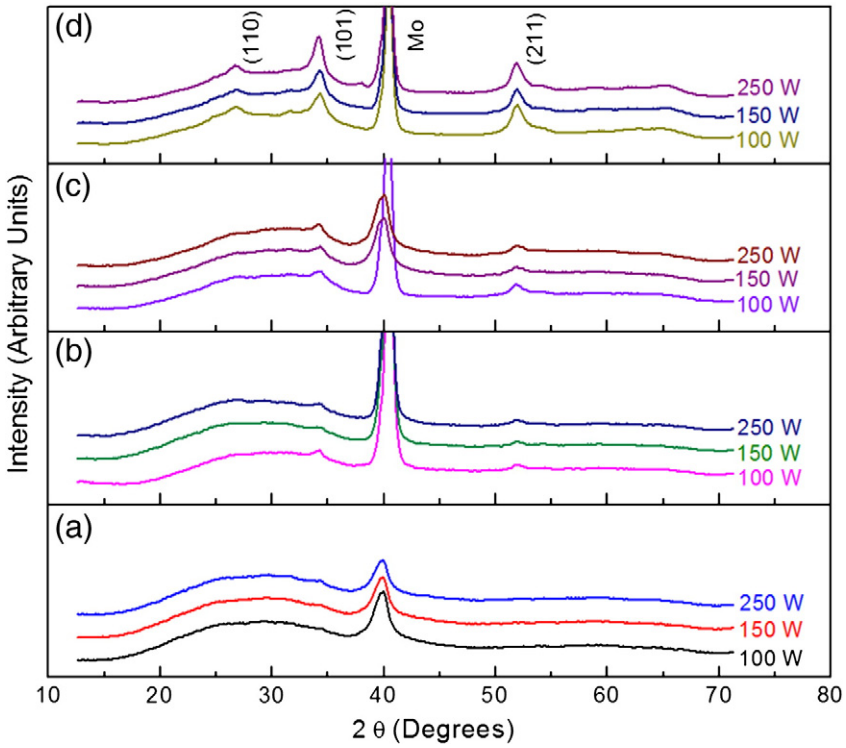

Fig. 2. X-ray diffraction pattern from SnO_2 films deposited using different RF sputtering powers. XRD from 200 nm thick SnO_2 films deposited (a) at room temperature and (b) at 150 °C. XRD from 500 nm thick SnO_2 films deposited (c) at room temperature and (d) at 150 °C. The SnO_2 diffractions are labeled with Miller indices whereas the Mo (110) peak at 40.5° is labeled as Mo.

(b), show amorphous diffraction pattern with very weak (101) and (211) peaks, while the 500 nm films show distinct (101) and (211) peaks, Fig. 2(c) and (d). Second, increasing the substrate temperature from room temperature to 150 °C also increases crystallinity. In Fig. 2(d), which shows the XRD from a 500 nm thick film deposited at 150 °C, the (110), (101) and (210) peak intensities are all much more intense than those in Fig. 2(c), the XRD for a 500 nm thick film deposited at room temperature. Third, increasing the RF plasma power also appears to increase the crystallinity, though this effect is much less obvious than the changes due to film thickness and substrate temperature.

Fig. 3 shows the scanning electron micrograph (SEM) of the 500 nm thick SnO_2 film deposited using 250 W RF power at 150 °C. The film was grown on (100) Si substrates. The columnar grains of the film are aligned along the (101) plane normal to the (100) Si surface. As it is clear from the SEM micrograph, the deposited film is smooth and continuous over the substrate. Other films also showed similar characteristics.

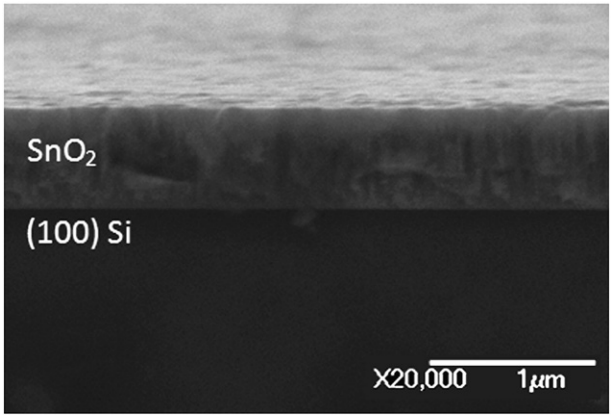

Fig. 3. Scanning electron micrograph of SnO_2 films deposited on Si (100) substrates at 250 W RF power and at 150 °C.

The broad diffraction spanning the range 20° to 37° is present on films deposited on all the substrates (SLG, Mo-SLG and (100) Si) and increases with increasing SnO_2 thickness suggesting that it is due to SnO_2. Such broad diffraction can originate from amorphous glasses. We attribute absence of sharper diffractions but presence of this broad peak to the presence of amorphous SnO_2 in the film. Thus, we conclude that thin (200 nm or less) films deposited at low RF powers and low temperatures tend to contain amorphous SnO_2 but the film crystallinity increases with increasing film thickness, substrate temperature and RF power. Whether crystalline regions exist in films deposited at room temperature and in 200 nm thin films cannot be concluded from XRD alone. The diffraction peak from the nanocrystals overlaps with the broad amorphous feature. To address this issue we examined the films using cross sectional TEM. We found that the 200 nm thick films deposited at room temperature consisted of 5–10 nm SnO_2 nanocrystals embedded in an amorphous SnO_2 matrix. The nanocrystals are surrounded by amorphous SnO_2 and do not abut against each other. Thus, despite its nanocrystalline structure the films do not contain any grain boundaries. Fig. 4(a) and (b) shows high-resolution TEM images of the SnO_2 films grown using 250 W RF at room temperature and 250 W RF at 150 °C. These films were deposited on native oxide covered Si substrates to facilitate TEM while approximating deposition on glass substrates. The selected area electron diffraction (SAED) patterns obtained from the films confirm the presence of both amorphous and crystalline components in both films. The film grown using 250 W RF at 150 °C exhibits more intense polycrystalline-like diffraction ring indicative of higher crystalline content than that of 250 W RF at room temperature.

The grain sizes, determined from the full width at half maximum of the XRD peaks using Scherer analysis are shown in Fig. 5 as a

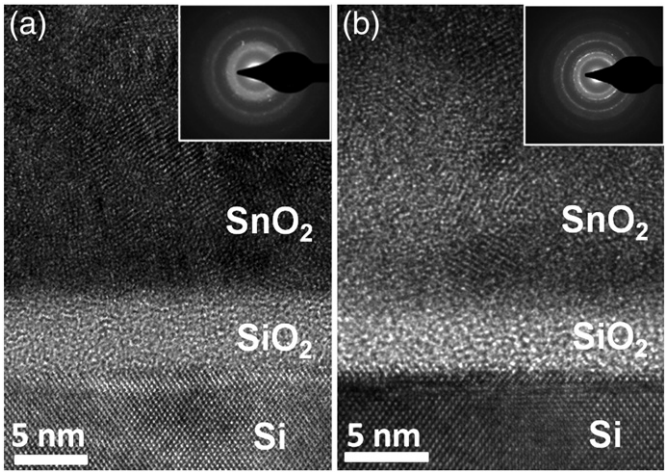

Fig. 4. High resolution TEM image of SnO_2 films deposited on Si/SiO_2 substrate using 250 W RF power at room temperature (a) and at 150 °C (b). The insets show the SAED patterns obtained from approximately 4×10^{-3} μm^3 volume of the films.

function of RF power for different substrate temperatures and film thicknesses. These grain sizes are consistent with the range of grain sizes observed using TEM. The grain size is a strong function of the SnO_2 film thickness suggesting that SnO_2 crystals nucleate and grow during deposition. It seems that the films start out amorphous and SnO_2 crystallites nucleate and grow as the deposition proceeds. Grains are also larger at 150 °C substrate temperature than at room temperature.

Table 1 lists the electrical resistivity, the carrier mobility and the carrier density of the SnO_2 films deposited on glass substrate. The resistivity of the films decreases with increasing RF power. This decrease is partially due to an increase in the carrier concentration and partially due to an increase in the mobility. The general trend in increasing mobility may be explained by better film crystallinity at higher RF powers. While it is possible that this increase may be brought about by unintentional heating of the substrate at higher sputtering powers, the platen temperature did not rise during sputtering. Increasing carrier concentration with RF power indicates an increase in the concentration of defects that dope SnO_2 n-type. These are thought to be O-vacancies [8]. Temperature is the other deposition parameter that affects the resistivity. Increasing the temperature can affect the film resistivity in two ways. First, increasing the

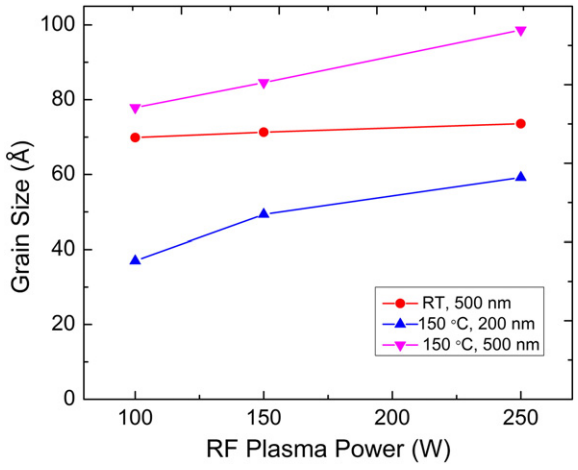

Fig. 5. Grain size in SnO_2 films deposited on Mo-coated SLG substrates estimated from Scherer analysis.

Table 1
Electrical resistivity, carrier concentration and hall mobility of the SnO_2 films sputtered under different RF powers and with different thicknesses.

RF Power	Thickness	Temp.	ρ (Ω cm)	n (x 10^{19} cm^{-3})	μ (cm^2/V s)
100 W	200 nm	Room temp.	N/A	N/A	N/A
150 W	200 nm	Room temp.	0.70	N/A	N/A
250 W	200 nm	Room temp.	0.16	3.6	1.1
100 W	500 nm	Room temp.	0.25	N/A	N/A
150 W	500 nm	Room temp.	0.20	5.7	0.5
250 W	500 nm	Room temp.	0.009	16.3	4.5
100 W	200 nm	150 °C	0.35	N/A	N/A
150 W	200 nm	150 °C	0.17	4.2	0.9
250 W	200 nm	150 °C	0.011	8.9	6.5
100 W	500 nm	150 °C	0.77	1.8	0.4
150 W	500 nm	150 °C	0.05	3.2	3.9
250 W	500 nm	150 °C	0.008	35.9	2.1

temperature can increase the crystallinity and improve mobility, which would decrease the resistivity. On the other hand, increasing the temperature can anneal oxygen vacancies and defects, which are thought to dope the film [8]. This, in contrast, would increase the resistivity. For example, the carrier concentration decreases from $5.7\times\times10^{19}$cm^{-3} to 3.2×10^{19}cm^{-3} when the deposition temperature is increased from room temperature to 150 °C for the 500 nm thick film deposited using 150 W RF power. These effects compete to determine the film resistivity and which trend dominates depend on other deposition parameters. Indeed, depending on the rf power we observe both trends in resistivity. Focusing on 500 nm thick films deposited at 100 W, we observe that the film resistivity increases (from 0.25 Ω cm to 0.77 Ω cm) as the temperature is increased from room temperature to 150 °C. In contrast, the resistivity of the films deposited at higher RF powers decrease with increasing deposition temperature. In general, mobilities increase with increasing deposition temperature. The lower mobility for the highest conductivity film deposited at 250 W and 150 °C may be due to scattering from the high concentration of defects that dope the films. Indeed, the carrier concentration of this film is very high.

3.2. Effect of the film thickness on electrical and structural properties

Fig. 6 shows the effect of film thickness on the XRD patterns from SnO_2 films deposited at room temperature, Fig. 6(a), and at 150 °C, Fig. 6(b). This figure clearly shows the effect of the deposition time on the films' crystallinity. The 200 nm thick films deposited at room temperature exhibit mostly an amorphous diffraction pattern whereas thicker films begin to show larger XRD peaks from (101) planes. The XRD peaks are larger partly because there is more material in thicker films. Indeed, TEM shows that even the 200 nm thick films contain nanocrystals embedded in amorphous SnO_2. However, the intensity of the diffraction from the (101) planes relative to the broad diffraction from amorphous tin dioxide also increases with film thickness indicating that the film structure becomes more crystalline. The effect of film thickness on the film structure is most obvious for films deposited at 150 °C as the intensity of the (101) XRD peak increases steadily as the film thickness increases from 200 nm to 500 nm. Also, Fig. 5 shows that the crystal sizes in thicker films are substantially larger.

Fig. 7(a) and (b) shows the resistivity, the mobility and the carrier density in SnO_2 films as a function of thickness at room temperature and at 150 °C, respectively. As the films get thicker, the film resistivity decreases but reaches a constant value. At room temperature, this decrease is due to an increase in higher carrier concentration because mobility remains approximately constant at 1–2 cm^2/V s. At 150 °C, the decrease in resistivity is mainly due to an increase in mobility while the carrier concentration remains constant with film thickness.

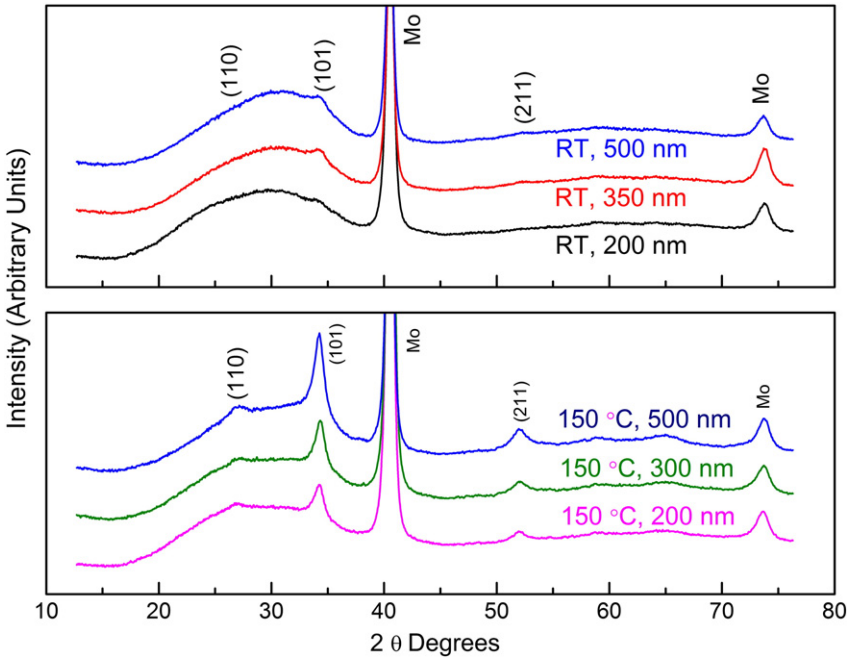

Fig. 6. X-ray diffraction from different thickness SnO_2 films deposited on Mo-coated SLG substrates (a) at room temperature, (b) at 150 °C using 250 W RF sputtering power.

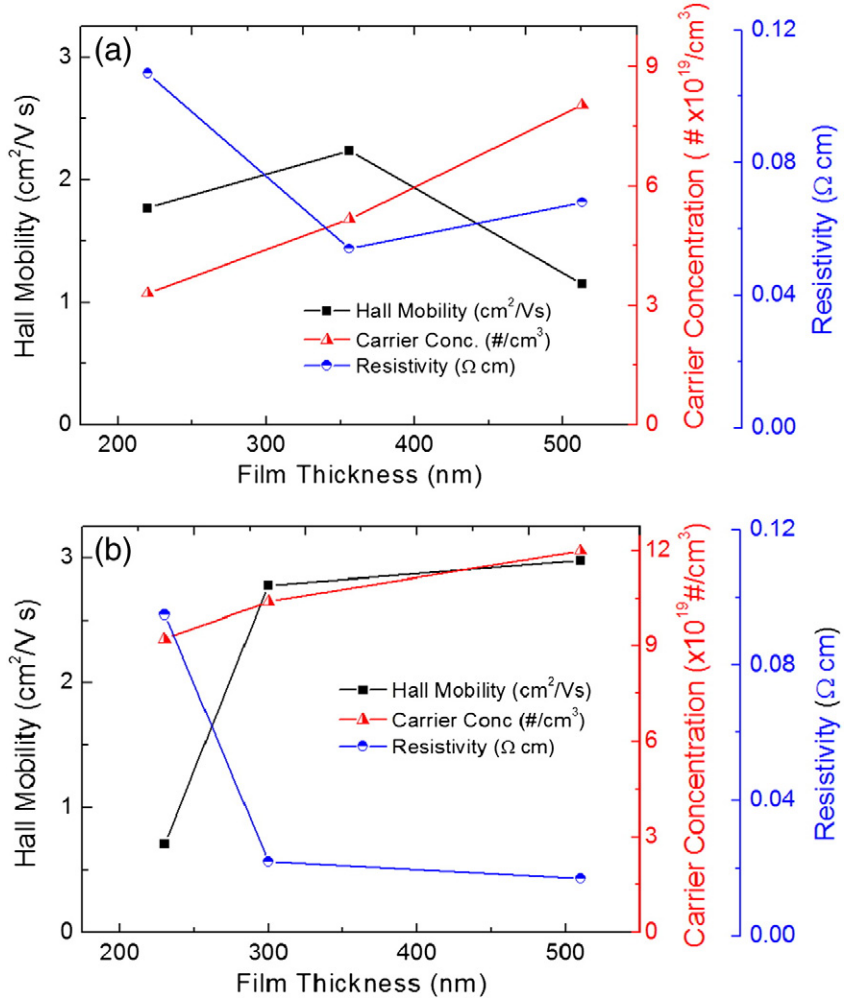

Fig. 7. Electrical resistivity, carrier concentration and Hall mobility of SnO_2 films on SLG substrates as a function of film thickness. Films were deposited (a) at room temperature and (b) at 150 °C using 250 W RF sputtering power.

The mobility in the film deposited at 150 °C is higher as expected. These trends are consisted with the XRD data shown in Fig. 6: thinner films consist of nanocrystals embedded in amorphous SnO_2 and mobility is approximately at 1–2 cm^2/V s. In contrast at 150 °C, the mobility increases due to higher film crystallinity.

3.3. Effect of O_2 concentration in the feed gas on electrical and structural properties

Fig. 8 shows the effect of O_2 concentration in the feed gas on the SnO_2 deposition rate. During the experiments, the RF power was kept constant at 250 W. These films were approximately 350 nm thick. The O_2 concentration in the feed gas was varied between 0% and 15%. Only a slight decrease in deposition rate is observed when O_2 concentration is increased beyond 10% but the deposition rate remains approximately constant up to 10% O_2 addition.

Fig. 9(a) and (b) shows the effect of O_2 concentration in the feed gas on the crystallinity of the films deposited on Mo-coated SLG and (100) Si wafers, respectively. The films were deposited at room temperature using 250 W RF power. As the O_2 concentration in the feed gas increases, the intensity of the (110), (101) and (211) XRD peaks increase indicating that the films become more crystalline. Films deposited at low O_2 concentrations show that XRD from (101) planes is dominant despite the fact that (110) diffractions should be the largest for a powder diffraction pattern. The films deposited at low O_2 mole fractions show that films are textured with (101) planes oriented normal to the substrate surface but the intensity of the (110) peak grows steadily with increasing O_2 concentration. When the O_2 concentration in the chamber reaches 10%, the film structure changes from a textured film where the [101] axis of the grains are oriented normal to the surface to more randomly oriented grain structure. A continuous increase in the (211) peak intensity with increasing O_2% in the feed gas is also observed. In contrast, at high O_2 concentrations in the feed gas, the deposited film XRD shows an intensity distribution closer to the powder diffraction pattern.

Clearly, the mobility is determined by the microstructure and orientation of the grains. Fig. 10 shows the resistivity, the mobility and the carrier concentration in SnO_2 films deposited at room temperature using 250 W RF power. The resistivity increases as O_2 concentration in the feed gas increases. This is partially due to decreasing mobility and partially due to decreasing carrier concentration. The decrease in carrier concentration is attributed to the reduction in O-vacancies with increasing O_2 in the feed gas. With small addition of

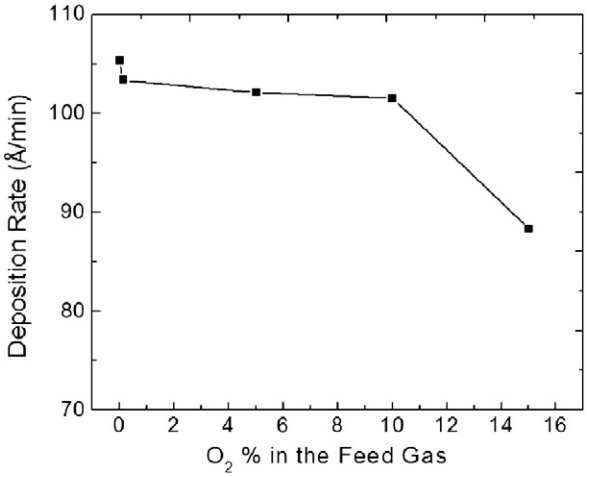

Fig. 8. Average deposition rates of SnO_2 films as a function of O_2% in the feed gas. Films were 350 nm thick and were deposited using 250 W RF sputtering power.

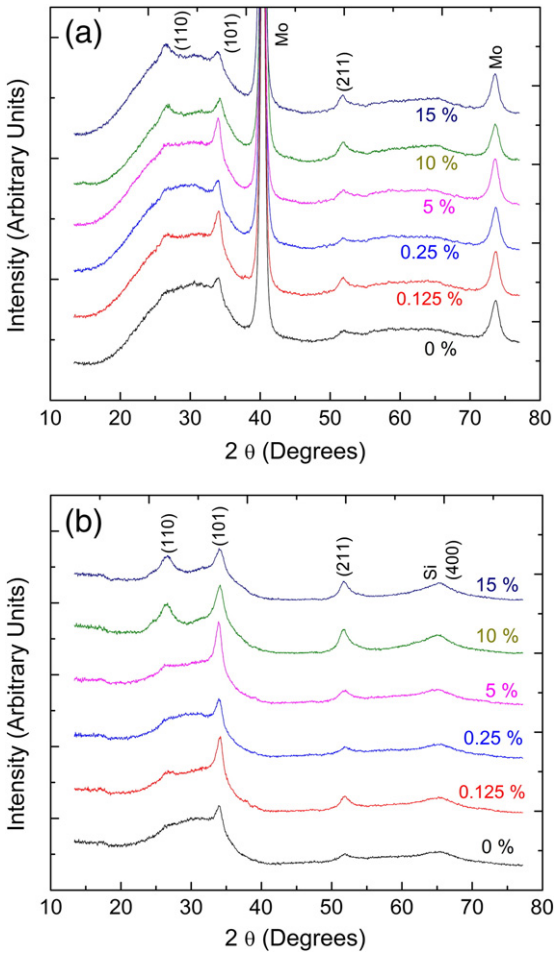

Fig. 9. X-ray diffraction from the SnO_2 films deposited using different O_2% in the feed gas (a) on Mo-coated SLG substrates and (b) on (100) Si substrates.

O_2, the film crystallinity improves as revealed by the increasing XRD peak along the (101) direction. Thereafter the carrier mobility decreases with O_2 concentration because the films become less textured: the (110) XRD peak grows in as the (101) XRD peak decreases. The film's XRD pattern becomes more like that of a powder diffraction pattern. As the O_2 concentration in the feed gas is increased above 10%, the preferred orientation of the film changes from (101) to (110) and the mobility begins to increase again as the film become textured again, albeit in another direction (110).

3.4. Optical properties

Figs. 11 and 12 show the optical transmission and Tauc plots for SnO_2 films, respectively. The films were transparent in the visible region of the optical spectrum but begin to absorb below ~400 nm. The extrapolation of Tauc plots yielded band gaps ranging from 3.4 eV to 3.65 eV. While there is a systematic increase in the band gap with decreasing sputtering power, the Tauc extrapolation method is sensitive to the details of the extrapolation and accurate to about 0.1 eV. The small differences (~0.05 eV) between 200 nm and 500 nm thick films are within the accuracy of the Tauc method: the band gap should not be a function of the film thickness. Band gap of SnO_2 has been suggested to shift to lower values than 3.6 eV with increasing oxygen vacancies [21]. This hypothesis is consistent both with our optical and electrical characterization data. Increasing the sputtering power decreases the band gap and carrier concentration and both of

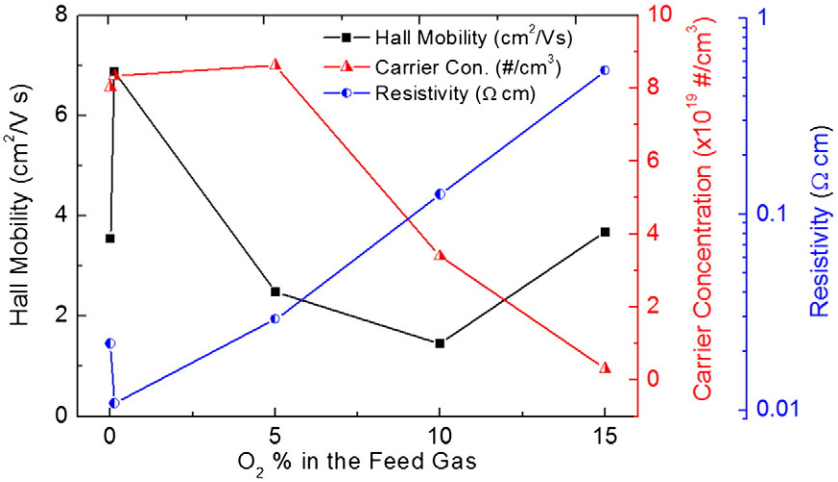

Fig. 10. The resistivity, the carrier concentration and the Hall mobility of SnO_2 films on SLG substrates as a function of O_2% in the feed gas.

these effects have been hypothesized to be due to increasing oxygen vacancies in the film [8,21]. The index of refraction extracted from the visible (500–700 nm) transmission using methods described in reference 22 ranged between 1.8 and 1.9. This is slightly lower than the index of refraction of bulk SnO_2[22] and we attribute this lower value to internal voids, which were also observed in low-resolution TEM images.

4. Conclusions

Sputtered SnO_2 films become more crystalline with increasing RF power, film thickness and substrate temperature. A small amount of O_2 (0.125%) in the feed gas also increases the crystallinity of the films. The SnO_2 film electrical resistivity decreases with increasing RF power, film thickness and substrate temperature. The lowest resistivity, 8 mΩ cm, is achieved at 150 °C and using 250 W RF power in a 500 nm thick film. The highest carrier concentration, 3.6×10^{20} cm^{-3}, is achieved with 250 W RF power and 150 °C substrate temperature in 500 nm thick SnO_2 films. A decrease in carrier concentration from 10^{20} cm^{-3} to 10^{18} cm^{-3} is observed when O_2 is added into the feed gas. The carrier mobility of the films increases with increasing RF power, film thickness and substrate temperature. Semicrystalline SnO_2 thin films can have mobilities of the order of 1–3 cm^2/Vs. This is only slightly lower than the mobilities achieved in polycrystalline SnO_2 and ZnO films (5–35 cm^2/Vs) [23–27] and our highest crystallinity films deposited by sputtering (6.8 cm^2/Vs). We recently showed that the semicrystalline films have superior water barrier properties as compared to polycrystalline SnO_2 and ZnO films. We were also able to assemble CIGS solar cells with semicrystaline SnO_2 films with no sacrifice in the solar cell efficiency as compared to films made with polycrystalline ZnO: these results will be reported elsewhere. Thus, while there is some sacrifice in the carrier mobility of the semicrystalline SnO_2 films in comparison to polycrystalline SnO_2 and ZnO, it is not significant to cause degradation of device

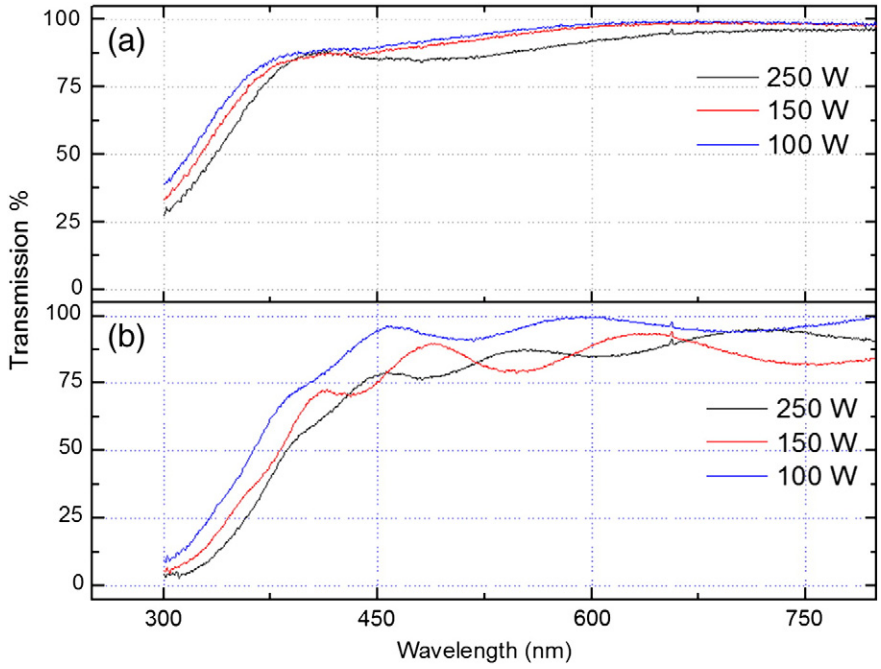

Fig. 11. Optical transmission of nominally (a) 200 nm and (b) 500 nm thick SnO_2 films sputtered at various RF powers at room temperature.

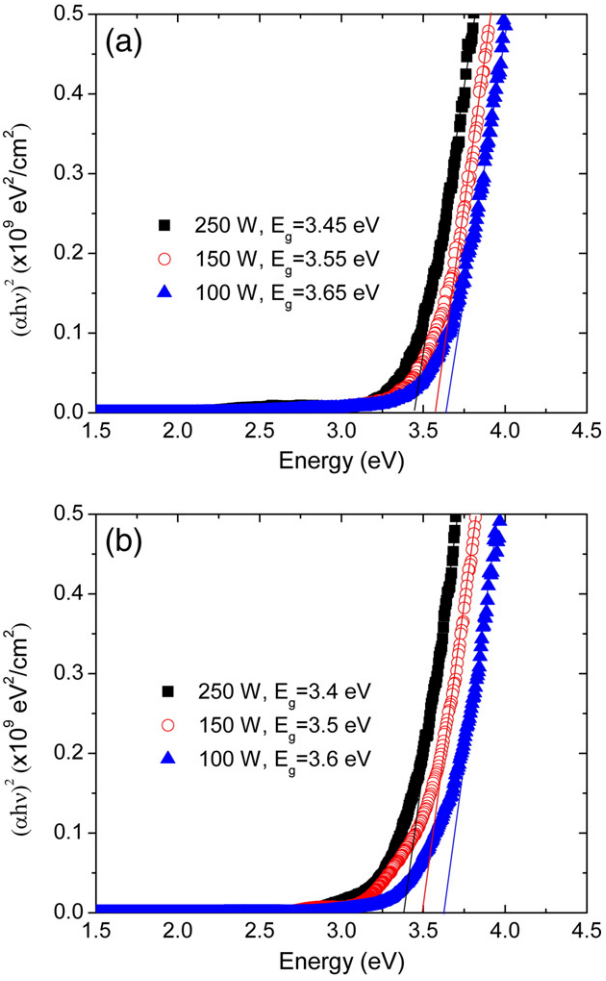

Fig. 12. Tauc plots for (a) 200 nm and (b) 500 nm thick SnO_2 films sputtered at various rf powers at room temperature. Extrapolated values of the band gap are in the legend.

characteristics. However, their barrier penetration properties are significantly improved. At the 150 °C substrate temperature, 250 W RF power and 500 nm thick films, the carrier mobility is achieved lower than what is expected. This is attributed to increasing defect scattering with increasing carrier density. The highest carrier mobility is achieved as 6.8 $cm^2/V\,s$ with 250 W RF power and 350 nm thick films with 0.125% of O_2 in the feed gas. While the trends discussed above are reproducible, the absolute values are sensitive to chamber base pressure, sputtering target and sputtering target age. For example, the films in Table 1 and Fig. 7 were deposited using different targets.

Acknowledgements

This work was funded by the Dow Chemical Company and by the Initiative for Renewable Energy and the Environment program of the University of Minnesota (IREE grant M7-2008). This work utilized the University of Minnesota Characterization Facility, which receives partial support from the NSF-NNIN program and capital equipment funding from the NSF through the MRSEC program DMR-0819885. A. Gunawan was supported by the NSF through the MRSEC program DMR-0819885.

References

[1] M.A. Gubbins, V. Casey, S.B. Newcomb, Thin Solid Films 405 (2002) 270.
[2] A. Martel, F. Caballero-Briones, P. Bartolo-Perez, A. Iribarren, R. Castro-Rodrigues, A. Zapata-Navarro, J.L. Pena, Surf. Coat.Technol. 148 (2001) 103.
[3] T.W. Kim, Mater. Res. Bull 36 (2001) 349.
[4] T.W. Kim, D.U. Lee, M. Jung, J.H. Lee, D.C. Choo, J.W. Cho, K.Y. Seo, Y.S. Yoon, Appl. Surf. Sci. 182 (2001) 69.
[5] W.C. Chang, S. Lee, X. Qi, J. Electrochem. Soc. 157 (2010) J245.
[6] S. Jager, B. Szyszka, J. Szczyrbowski, G. Brauer, Surf. Coat.Technol. 98 (1998) 1304.
[7] S.U. Lee, B. Hong, W.S. Choi, J. Vac. Sci. Technol. A 27 (2009) 996.
[8] J. Montero, J. Herrero, C. Guillen, Sol. Energy Mater. Sol. Cells 94 (2010) 612.
[9] V. Senthilkumar, P. Vickraman, J.J. Prince, M. Jayachandran, C. Sanjeeviraja, Phil. Mag. Lett. 90 (2010) 337.
[10] C. Korber, P. Agoston, A. Klein, Sensor Actuat. B-Chem. 139 (2009) 665.
[11] T. Diana, K.N. Devi, H.N. Sarma, Indian J. Phys. 84 (2010) 687.
[12] T.P. Niesen, M.R. De Guire, Solid State Ionics 151 (2002) 61.
[13] S.G. Ansari, M.A. Dar, M.S. Dhage, Y.S. Kim, Z.A. Ansari, A. Al-Hajry, H. Shin, Rev. Sci. Intrum. 80 (2009) 0451121.
[14] T. Serin, N. Serin, S. Karadeniz, H. Sari, N. Tugluoglu, O. Pakma, J. Non-Cryst. Solids 352 (2006) 209.
[15] X.Q. Pan, L. Fu, J. Appl. Phys. 89 (2001) 6048.
[16] M. Alaf, M.O. Guler, D. Gultekin, M. Uysal, A. Alp, H. Akbulut, Vacuum 83 (2009) 292.
[17] S.S. Pan, G.H. Li, L.B. Wang, Y.D. Shen, Y. Wang, T. Mei, X. Hu, Appl. Phys. Lett. 95 (2009) 222112.
[18] C. Korber, J. Suffner, A. Klein, J. Phys. D: Appl. Phys. 43 (2010) 055301.
[19] H.L. Ma, X.T. Hao, J. Ma, Y.G. Yang, J. Huang, D.H. Zhang, X.G. Xu, Appl. Surf. Sci. 191 (2002) 313.
[20] M.J. Behr, K.A. Mkhoyan, E.S. Aydil, ACS Nano 4 (2010) 5087.
[21] C. Drake, S. Seal, Appl. Phys. Lett. 90 (2007) 233117.
[22] J.C. Manifacier, M. De Murcia, J.P. Pillard, Thin Solid Films 41 (1977) 127.
[23] J. Bruneaux, H. Cachet, M. Froment, A. Messad, Thin Solid Films 197 (1991) 129.
[24] S. Shirakata, A. Yokoyama, S. Isomura, Jpn. J. Appl. Phys. 2 (35) (1996) L722.
[25] R.Y. Korotkov, A.J.E. Farran, T. Culp, D. Russo, C. Roger, J. Appl. Phys. 96 (2004) 6445.
[26] A. Oprea, E. Moretton, N. Barsan, W.J. Becker, J. Wollenstein, U. Weimar, J. Appl. Phys. 100 (2006) 033716.
[27] B.S. Sang, Y. Nagoya, K. Kushiya, O. Yamase, Sol. Energy Mater. Sol. Cells 75 (2003) 179.